Metabolic Brain Disease (2021) 36:2071–2078
https://doi.org/10.1007/s11011-021-00782-9

ORIGINAL ARTICLE

Differential involvement of hippocampal subfields in Niemann-Pick type C disease: a case–control study

Pierre Wibawa[1,2] · Florian Kurth[3] · Eileen Luders[3,4] · Christos Pantelis[1,5] · Vanessa L. Cropley[1] · Maria A. Di Biase[1,6] · Dennis Velakoulis[1,2,5] · Mark Walterfang[1,2,5]

Received: 15 February 2021 / Accepted: 7 June 2021 / Published online: 19 June 2021

Abstract

Hippocampal brain regions are strongly implicated in Niemann Pick type C disease (NPC), but little is known regarding distinct subregions of the hippocampal complex and whether these are equally or differentially affected. To address this gap, we compared volumes of five hippocampal subfields between NPC and healthy individuals using MRI. To this end, 9 adult-onset NPC cases and 9 age- and gender-matched controls underwent a 3 T T1-weighted MRI scan. Gray matter volumes of the cornu ammonis (CA1, CA2 and CA3), dentate gyrus (DG), subiculum, entorhinal cortex and hippocampal-amygdalar transition area were calculated by integrating MRI-based image intensities with microscopically defined cytoarchitectonic probabilities. Compared to healthy controls, NPC patients showed smaller volumes of the CA1-3 and DG regions bilaterally, with the greatest difference localized to the left DG (Cohen's $d = 1.993$, $p = 0.008$). No significant associations were shown between hippocampal subfield volumes and key clinical features of NPC, including disease duration, symptom severity and psychosis. The pattern of hippocampal subregional atrophy in NPC differs from those seen in other dementias, which may indicate unique cytoarchitectural vulnerabilities in this earlier-onset disorder. Future MRI studies of hippocampal subfields may clarify its potential as a biomarker of neurodegeneration in NPC.

Keywords Niemann-Pick Type C · Hippocampus · Hippocampal Subfields · Magnetic resonance imaging

Introduction

Niemann-Pick disease type C (NPC) is a metabolic disorder that is inherited in an autosomal recessive manner and involves disruptions to intracellular endo-lysosomal cholesterol trafficking. In 95% of cases, the disease is attributed to pathogenic variants in the NPC1 gene on chromosome 18q11-q12, while the remaining 5% of cases are associated with the NPC2 gene on chromosome 14q24.3 (Patterson 1993). The annual incidence of NPC ranges between 0.25 and 2.25 in 100,000 live births (Geberhiwot 2018). Clinical presentations vary markedly from infancy to mid-adulthood, but typical manifestations often feature ataxia, dystonia, gelastic cataplexy, vertical supranuclear ophthalmoplegia, psychotic and mood disorders, hepatosplenomegaly, and progressive cognitive impairment (Geberhiwot et al. 2018; Sevin et al. 2007). On a biochemical screening test, the majority of patients show elevated plasma oxysterol levels. Intracellular accumulation of unesterified cholesterol can also be observed with Filipin staining in cultured fibroblasts. However, this confirmatory investigation is increasingly superseded by gene panel test or sequencing. Findings on structural magnetic resonance imaging (MRI) can be variable, but significant gray matter atrophy has been reported, particularly in the cerebellum, thalamus, dorsal striatum, and medial temporal lobe, in addition to widespread alterations in white matter (Walterfang 2010; Walterfang 2013).

✉ Pierre Wibawa
pierre.wibawa@gmail.com

1 Melbourne Neuropsychiatry Centre, University of Melbourne, Parkville, Victoria, Australia

2 Neuropsychiatry, Royal Melbourne Hospital, Parkville, Victoria, Australia

3 School of Psychology, University of Auckland, Auckland, New Zealand

4 Laboratory of Neuro Imaging, School of Medicine, University of Southern California, Los Angeles, CA, USA

5 Florey Institute of Neuroscience and Mental Health, Parkville, Victoria, Australia

6 Psychiatry Neuroimaging Laboratory, Harvard Medical School, Boston, MA, USA

Alterations of the hippocampi (within the medial temporal lobes [MTL]) are particularly notable in NPC given the substantial overlap of this neuropathological feature with other neurodegenerative diseases (Rego 2019). In addition to features consistent with many lysosomal storage disorders, including swollen axonal hillocks, meganeurites, and axonal spheroids, NPC brains demonstrate extensive accumulation of hyperphosphorylated tau and neurofibrillary tangles (NFT), as well as altered amyloid processing albeit without plaque formation (Walterfang et al. 2013; Zhang et al. 2010). In Alzheimer's disease (AD), pathogenic tau deposition is an established marker of disease progression, where NFT can be observed initially in the entorhinal region of MTL and later across the hippocampal subfields (Braak et al. 2006). The extent and pattern of pathogenic spread in the hippocampi of individuals with NPC are less known. Nonetheless, increased abnormal tau has been found in the MTL regions of NPC patients using positron emission tomography (PET) imaging (Villemagne et al. 2019). Furthermore, non-specific regional alterations have been observed in an MRI shape analysis of the hippocampus bilaterally and in post-mortem studies (Walterfang et al. 2013; Zhang et al. 2010).

While preliminary evidence implicates the hippocampal complex in NPC pathophysiology, differential effects across distinct hippocampal subfields remain unknown. We set out to investigate differences between adult NPC patients and matched healthy controls in the volumes of five hippocampal subfields: (i) CA1-3, (ii) dentate gyrus, (iii) subiculum, (iv) the adjoining entorhinal cortex; and (v) the hippocampal-amygdalar transition area (Amunts 2005). To calculate the gray matter volumes of these distinct subfields, we employed a novel approach combining microscopically defined cyto-architectonic probabilities with MRI-based image intensities (Kurth et al. 2015a, 2017b, c, 2018a, b; Luders et al. 2013). Based on previous results (Walterfang et al. 2013; Zhang et al. 2010), we hypothesized that NPC patients would have smaller whole hippocampi volumes relative to healthy controls; however, we refrained from making assumptions regarding specific subfields. In an additional exploratory analysis, we further tested for associations between gray matter volumes and clinical features, including disease duration, symptom severity and the presence of psychosis within the NPC group.

Material and methods

Participants

Nine cases of genetically-confirmed NPC and 9 age- and gender-matched healthy controls were included (Walterfang 2020). Diagnosis of NPC was confirmed with filipin staining and NPC1 genotyping. Iturriaga rating scale and onset of neurological symptom indicated illness severity and duration of illness, respectively (Iturriaga et al. 2006). A history of a psychotic disorder was also obtained from medical records. Healthy controls were recruited through advertisements and were excluded if they reported a personal or first-degree family history of a neurological or psychiatric illness or alcohol and substance dependence as inferred from the Structured Clinical Interview for DSM-IV Axis I Disorders (First et al. 2004). Individuals with a contraindication to MRI, previous head injury, impaired thyroid function, diabetes or pregnancy were also excluded from the study. Participant characteristics are shown in Table 1.

MR acquisition

T1-weighted 3D spoiled gradient recalled echo images were collected on a 3 Tesla Siemens Trio scanner with 32-channel coils at the Murdoch Children's Research Institute, Royal Children's Hospital, Parkville, Victoria. The acquisition parameters were 14 ms repetition time, 3 ms echo time, 256 contiguous slices and $1 \times 1 \times 1$ mm^3 voxel size. The MR acquisition and clinical assessments were performed blinded to the image pre-processing and data analyses.

Image pre-processing

All T1-weighted images were pre-processed using SPM12 (http://www.fil.ion.ucl.ac.uk/spm) and the CAT12 toolbox (http://dbm.neuro.uni-jena.de/cat/), as described previously (Kurth et al. 2015a, 2017b, c, 2018a, b; Luders et al. 2013). In short, images were corrected for magnetic field inhomogeneities, and then classified into gray matter (GM), white matter (WM), and cerebrospinal fluid (CSF) using partial volume estimation. Subsequently, the resulting GM segments were spatially normalized to the DARTEL template provided with the CAT12 toolbox (Ashburner 2007). The resulting normalized GM segments were finally divided by the linear and non-linear components of the Jacobian determinant derived from the normalization matrix to preserve the original amount of tissue per voxel (Ashburner and Friston 2000; Good et al. 2001; Kurth et al. 2015b). To account for differences in intracranial volume, the total intracranial

Table 1 Sample characteristics

	NPC Patients	Controls
Age (years)*	32.2 ± 11.8 [18 – 52]	31.9 ± 9.4 [18 – 42]
Sex	5 females / 4 males	5 females / 4 males
Disease duration (years)*	9.2 ± 3.1 [5 – 13]	-
Symptom severity score*	9.7 ± 3.9 [5 – 16]	-
Psychosis	$n = 2$	-

*Mean, standard deviation, and range are given

volume (TIV) was calculated by adding the volumes of the tissue classes in native space (TIV = GM + WM + CSF) to be later included as covariate in the statistical model.

Data analyses

To investigate differences between NPC patients and healthy controls in the hippocampal complex, we assessed the hippocampus as a whole (HIPPO) as well as across five subregions: cornu ammonis (CA1, CA2, and CA3), dentate gyrus (DG), subiculum (SUB) hippocampus-adjacent entorhinal cortex (EC) and hippocampal-amygdalar transition area (HATA). As detailed in Amunts et al. (2005), those subareas were originally established by first defining them in cell body-stained histological sections, followed by reconstruction in MNI single-subject space, and finally conversion into voxel-wise probabilities, see Fig. 1. As described in detail previously (Kurth et al. 2015a, 2017b, c, 2018a, b; Luders et al. 2013), these subarea-specific probability maps (Amunts et al. 2005), as provided by the Anatomy toolbox, version 2.2c (Eickhoff et al. 2005), were integrated with the preprocessed gray matter segments by voxel-wise multiplication. This voxel-wise integration yielded a probability-weighted measure of gray matter content (in mm^3) within the left and right hippocampal subareas as well as adjacent regions of the hippocampal complex. Gray matter content for the left and right hippocampus as a whole was calculated by summing the volumes of all subfields (HIPPO = CA1 + CA2 + CA3 + DG + SUB). The resulting means as well as adjusted means of the resulting volumes are provided in Table 2.

Statistical analyses were conducted in Matlab (The MathWorks, Natick, MA) using a mass-univariate general linear model (GLM). Specifically, the left and right volumes for HIPPO, CA1, CA2, CA3, DG, SUB, EC, and HATA were used as dependent variables, group as the independent variable, and age, sex, as well as TIV as covariates. Importantly, an assessment of the assumptions for parametric testing revealed a non-normal distribution of the residuals for left CA2 and left SUB as per a significant Lilliefors test. Thus, significance was assessed using a Monte-Carlo Simulation with 10,000 permutations. All results were corrected for multiple comparisons (across the 10 [five bilateral] subfields) by controlling the false discovery rate (FDR) at $p \leq 0.05$ (Benjamini and Yekutieli 2001; Hochberg and Benjamini 1990). Demographic and clinical measures were analyzed using either t-tests or chi-squared tests, according to data distribution.

In exploratory analyses, GLMs assessed associations between the subfields gray matter volumes and clinical features, including disease duration, symptom severity and history of psychosis in NPC patients only. These models used the left and right volumes for HIPPO, CA1, CA2, CA3, DG, SUB, EC, and HATA as dependent variables, disease duration, symptom severity, or psychosis as the respective independent variable, and age, sex, and TIV as covariates. Significance was assessed using Monte-Carlo Simulations with 10,000 permutations.

Results

Patients and controls did not differ in age (Cohen's $d = 0.034$, $t = 0.067$, $p = 0.947$) or sex (see Table 1). Within the patient group, there was no significant correlation between age and disease duration ($r = 0.396$, $p = 0.292$), between age and symptom severity ($r = -0.261$, $p = 0.498$), or between disease duration and symptom severity ($r = 0.184$, $p = 0.636$). Two NPC cases had a history of psychosis; however, these cases did not significantly differ

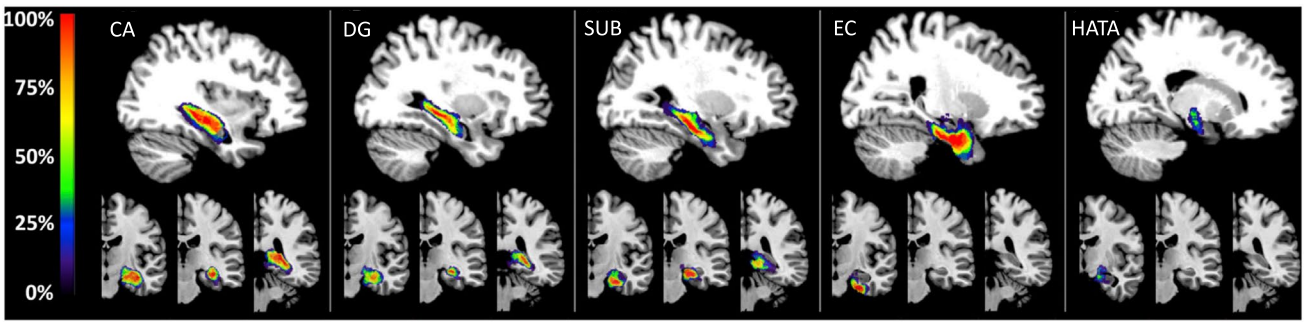

Fig. 1 Hippocampal subregions. Top Row: Cytoarchitectonically-derived probability maps of the cornu ammonis (CA), dentate gyrus (DG), subiculum (SUB), entorhinal cortex (EC), and hippocampal-amygdalar transition area (HATA), shown on sagittal sections of the MNI single-subject template. Note that the current study further distinguished CA into CA1, CA2, and CA3. Bottom Row: The same probability maps are displayed on the coronal sections, depicting the hippocampal head (left), body (middle), and tail (right). The color bar encodes the probability for each voxel to belong to the respective region. Reprinted and adapted from Kurth et al. (2017a) with permission from Elsevier

Table 2 Regional volumes of the hippocampal complex, including adjacent areas in mm^3 (mean ± SD)

	Region	Patients	Controls	Group difference**				
		Raw	Adjusted*	Raw	Adjusted*	Cohen's d	T-value	p-value
Left	HIPPO	2,639 ± 421	2,680 ± 213	3,018 ± 128	2,936 ± 125	1.439	2.595	0.016
	CA1	691 ± 104	692 ± 57	802 ± 56	775 ± 36	1.716	3.093	0.008
	CA2	229 ± 45	234 ± 26	275 ± 29	268 ± 31	1.150	2.074	0.032
	CA3	269 ± 45	276 ± 23	320 ± 24	314 ± 24	1.551	2.797	0.013
	DG	461 ± 67	473 ± 43	562 ± 41	553 ± 36	1.993	3.593	0.008
	SUB	989 ± 170	1,005 ± 85	1,059 ± 27	1,027 ± 58	0.298	0.537	0.193
	EC	964 ± 194	980 ± 112	1,078 ± 92	1,045 ± 93	0.629	1.133	0.112
	HATA	81 ± 18	82 ± 8	86 ± 8	82 ± 6	0.008	0.015	0.245
Right	HIPPO	2,632 ± 373	2,690 ± 204	3,007 ± 306	2,916 ± 171	1.178	2.123	0.031
	CA1	695 ± 105	709 ± 67	792 ± 72	770 ± 52	0.996	1.796	0.037
	CA2	281 ± 42	295 ± 25	334 ± 49	328 ± 36	1.051	1.895	0.032
	CA3	308 ± 44	317 ± 24	371 ± 49	361 ± 32	1.508	2.718	0.013
	DG	430 ± 60	437 ± 40	526 ± 58	511 ± 39	1.812	3.266	0.008
	SUB	918 ± 135	931 ± 66	984 ± 113	946 ± 64	0.219	0.395	0.204
	EC	1,123 ± 224	1,161 ± 134	1,231 ± 132	1,197 ± 111	0.288	0.518	0.193
	HATA	68 ± 12	68 ± 7	73 ± 13	69 ± 11	0.129	0.233	0.217
TIV	1,448 ± 112		1,365 ± 178					

For each region, raw volumes, as well as volumes adjusted for the mean TIV, age and gender, are presented

HIPPO whole hippocampus, *CA1-3* subareas 1–3 of the cornu ammonis, *DG* dentate gyrus, *SUB* subiculum, *EC* entorhinal cortex, *HATA* hippocampal-amygdala transition area, *TIV* total intracranial volume

*Adjusted for TIV, age, and sex

**FDR-corrected for multiple comparisons

from the others in terms of age (d = -0.169, T = -0.224, p = 0.829), disease duration (d = -0.269, T = -0.356, p = 0.733), or symptom severity (d = 0.244, T = 0.323, p = 0.757).

Controls had larger mean gray matter volumes than NPC patients in most hippocampal subfields. The group difference reached statistical significance for the whole hippocampus, CA1-3, and DG bilaterally. The largest effect was observed in the left DG (d = 1.993; T = 3.593; p = 0.008). There was no significant group difference in the subiculum, EC and HATA (pFDR > 0.05). Complete regional effect sizes, t-statistics and FDR-corrected p-values for all regions are shown in Table 2, and boxplots indicating the medians, quartiles, and 1.5 interquartile ranges are shown in Fig. 2.

Within the NPC group, gray matter volumes in the hippocampal and adjacent regions were not significantly associated with disease duration, symptom severity, or psychosis. When omitting the correction for multiple comparisons, there was a trend for an uncorrected positive association between symptom severity and gray matter volume in the left entorhinal cortex (r = 0.778, p = 0.056), and between disease duration and gray matter volume in the left CA3 (r = 0.772, p = 0.061), as well as a negative association between disease duration and gray matter volume in right HATA (r = -0.770, p = 0.060).

Discussion

We examined hippocampal subfields in adult NPC patients to determine if there was subfield-specific atrophy. In our cohort, the illness severity and duration (mean 9.2 years) corresponded to moderate disease stages of NPC, where we expect to observe reduced whole hippocampal volume accompanied by memory loss and other cognitive impairments (Bonnot et al. 2019; Heitz et al. 2017; Stampfer 2013; Walterfang et al. 2010; Walterfang et al. 2013). In this study, we found global and regional-specific hippocampal volume reductions in NPC patients compared to healthy controls. Regional effects were localized to the CA1-3 and the DG.

The marked reduction of DG and CA3 volume in the present study concurs with a pattern of tau deposition observed in previous post-mortem studies of NPC-affected brains (Distl et al. 2003; Zhang et al. 2010). NFTs in these regions have been reported across all age groups, including in children and adults (Distl et al. 2003; Zhang et al. 2010). Numerous NPC animal models also suggest early involvement of CA3-DG regions, where the boundary between the severely affected CA3-DG and relatively spared CA1 can be consistently demarcated at an early age (Treiber-Held et al. 2003; Zervas et al. 2001; Zhou et al. 2011). Besides tau, the affected neurons often show axonal spheroids, ectopic

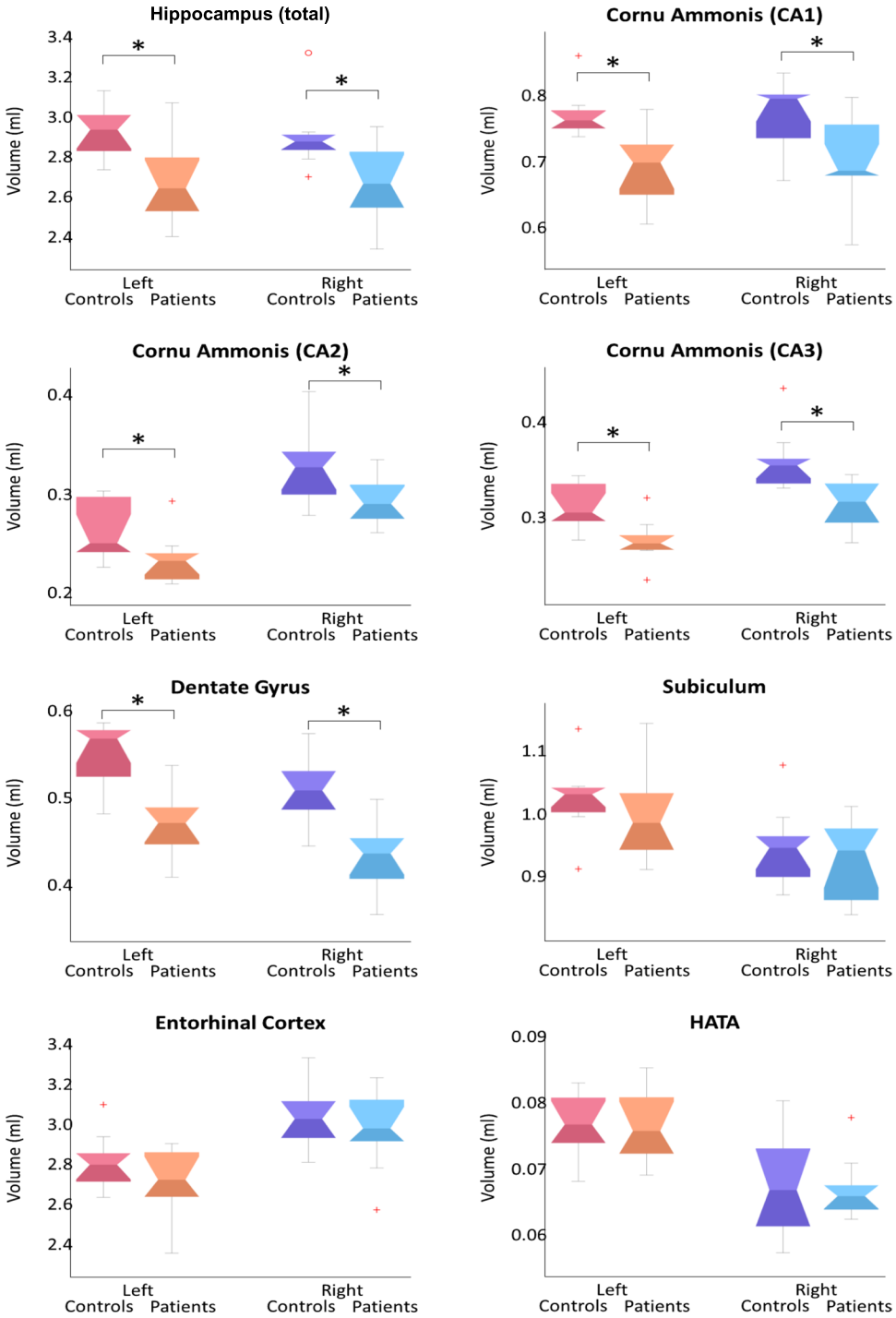

Fig. 2 Group differences within the hippocampal subfields and adjacent regions. The boxplots present the medians, quartiles, and 1.5 interquartile ranges (IQR) of the regional volumes, separately for controls and NPC patients, within each hemisphere (left-hemispheric volumes are shown on the left in red-spectrum colors, and right-hemispheric volumes on the right in blue-spectrum colors). Outliers beyond 1.5 IQR were denoted in red, '+' < 3 IQR < '0'. The volumes are adjusted for TIV, age, and sex (see Table 2). The asterisks (*) indicate significant group differences (controls > patients) FDR-corrected for multiple comparisons at $p \leq 0.05$

dendritogenesis, unesterified cholesterol, and GM3 gangliosides staining, which may underlie the volume reductions observed in the current study.

DG and CA3 are anatomically connected via mossy fibers (Kesner 2018). In healthy individuals, these structures continue to develop postnatally, as evidenced by mitotically active neurons. In NPC mouse model, higher mitotic activity in CA3 and DG than CA1 may assert greater metabolic demand, which subsequently amplifies the NPC pathogenic processes (Treiber-Held et al. 2003). Elsewhere, human cerebellar neurons, which are characteristically affected in NPC, are known to have high mitotic kinase cdc2/cyclin B1 activity with abnormal tau phosphorylation (Bu et al. 2002). Co-localization of mitotic epitope and NFT in the human hippocampi has also been observed in NPC (Zhang et al. 2010). Thus, abnormal tau phosphorylation, cholesterol

mistrafficking and elevated mitotic activity in NPC may synergistically accelerate neuronal damage in the CA3-DG region.

Neural dysconnectivity manifests globally in NPC and is seen across biological scales, ranging from cellular (synaptic structures) to macrostructural (brain volume) levels (Rego et al. 2019). Indeed, preliminary work has linked these findings across biological scales, such that dysconnectivity of the DG has been associated with DG atrophy in animal models of NPC. Following an injection of pseudorabies virus into the DG of NPC mice, the virus spreads and traces neuronal loss along its pathway, passing through CA2-3 and other subcortical regions (Byun 2011). A recent study implicates neuroinflammation via microglial activation as a potential mechanism underlying dysconnectivity in adult NPC patients (Walterfang et al. 2020). Clinically, widespread dysconnectivity and DG atrophy have been implicated in schizophrenia (Bora 2011; Nakahara et al. 2018; Tavitian et al. 2019), which may underpin the high incidence of schizophrenia-like psychosis in NPC (Bonnot et al. 2019; Rego et al. 2019). However, due to our small sample, we did not find any clinical associations with the subfields.

Reduced CA1 volume is also prominent in our NPC cohort. This is in line with a previous MRI study which observed hippocampal deformation in the CA1 region and widespread white matter alterations (Walterfang et al. 2013). Susceptibilities to tau-related pathology and glutaminergic excitotoxicity have been proposed in this region (Steve et al. 2014). Tauopathy in CA1 seems to present early in NPC patients. In a post-mortem study, the appearance of NFT and hyperphosphorylated tau in CA1 are found in children as young as 4 years old (Zhang et al. 2010). The involvement of CA1 also supports the view of prenatal neuronal damage in NPC, as this subfield and other cortical midline structure mature early in utero (Walterfang 2011). Besides tau, accumulation of amyloidogenic proteins is seen in CA1 NPC neurons (Causevic 2018). Clinically, early CA1 damage and its progression towards neighboring regions may predispose NPC patients to develop seizures and memory deficits (Bartsch 2015).

The absence of significant subiculum and EC changes in our NPC cohort contrasts with reports in AD populations, where early deposition of NFT in these regions are pathognomonic (Braak et al. 2006). This difference may be associated with the relative absence of amyloid plaque pathology and the young-onset nature of NPC (Causevic et al. 2018; Zhang et al. 2010). Reduced subicular volume is known to correlate with aging and conversion to dementia in the general population, MCI and Parkinson's disease (Evans 2018; Kurth et al. 2017a; Low et al. 2019; Mak 2019). Furthermore, as the volumes of subiculum and MTL have been correlated with the cerebrospinal fluid Aβ-amyloid level in conditions where amyloid plaques are common (i.e., AD, dementia with Lewy Bodies and Parkinson's disease), the absence of amyloid plaque in NPC may have spared the subiculum and EC (Mak et al. 2019; Muller-Ehrenberg et al. 2018; Stav 2016).

Several limitations are noteworthy, including our small sample size, which may have constrained power to detect associations between hippocampal volumes and NPC clinical measures (Walterfang et al. 2013). Furthermore, our macroscopic MRI analysis cannot capture distinct cellular and molecular processes underlying atrophy in NPC patients. To disentangle the influence of different patho-molecular processes in NPC, future studies could examine cerebrospinal fluid and radionucleotide imaging biomarkers for tau, Aβ-amyloid, neurofilament-light and microglial activation (Eratne et al. 2019; Mattsson 2012; Villemagne et al. 2019; Walterfang et al. 2020). As these biomarkers may precede atrophy (reduced hippocampal volume), their incorporation could be complemented by longitudinal evaluation of hippocampal subfields (Henneman 2009).

Conclusions

Overall, our case–control study has revealed an extensive pattern of hippocampal atrophy in NPC that is consistent with previous MRI and post-mortem studies. Despite NPC having a similar molecular pathogenic mechanism to AD and other neurodegenerative diseases, the regional pattern of hippocampal subfield involvement differs in NPC, which may indicate unique cytoarchitectural vulnerabilities. Regardless of the precise mechanisms, MRI-based measures of hippocampal subfields may serve as a potential biomarker of neurodegeneration in NPC.

Authors' contributions PW was involved in the conception and coordination of the study, as well as interpretation of the data. MW led the conception and coordination of the study. Image pre-processing and statistical analyses were conducted by EL and FK. PW led the manuscript preparation and writing of first draft along with EL, FK and MW. VC, MDB, CP and DV were involved in the conception, design and execution of the study, interpretation of data, review and critique of the draft. All authors approved of the manuscript's final version.

Funding The authors declared no specific grant for this research from any funding agency in public, commercial or not-for-profit sectors.

Data availability The generated and analyzed data during this study are available from the corresponding author on reasonable request.

Declarations

Ethical approval All procedures performed in this study were in accordance with the ethical standards of the Austin Health and Melbourne Health ethics committees (approval number 2012.066), Victo-

ria, Australia, and with the Australian National Statement on Ethical Conduct in Human Research (2007).

Informed consent Written informed consent was obtained from all individual participants included in the study.

Conflicts of interest None to declare.

References

Amunts K et al (2005) Cytoarchitectonic mapping of the human amygdala, hippocampal region and entorhinal cortex: intersubject variability and probability maps. Anat Embryol (berl) 210:343–352. https://doi.org/10.1007/s00429-005-0025-5

Ashburner J (2007) A fast diffeomorphic image registration algorithm. Neuroimage 38:95–113. https://doi.org/10.1016/j.neuroimage.2007.07.007

Ashburner J, Friston KJ (2000) Voxel-based morphometry–the methods. Neuroimage 11:805–821. https://doi.org/10.1006/nimg.2000.0582

Bartsch T et al (2015) Selective neuronal vulnerability of human hippocampal CA1 neurons: lesion evolution, temporal course, and pattern of hippocampal damage in diffusion-weighted MR imaging. J Cereb Blood Flow Metab 35:1836–1845. https://doi.org/10.1038/jcbfm.2015.137

Benjamini Y, Yekutieli D (2001) The control of the false discovery rate in multiple testing under dependency. Ann Statist 29:1165–1188. https://doi.org/10.1214/aos/1013699998

Bonnot O, Klünemann H-H, Velten C, Torres Martin JV, Walterfang M (2019) Systematic review of psychiatric signs in Niemann-Pick disease type C. World J Biol Psychiatry 20:320–332. https://doi.org/10.1080/15622975.2018.1441548

Bora E et al (2011) Neuroanatomical abnormalities in schizophrenia: a multimodal voxelwise meta-analysis and meta-regression analysis. Schizophr Res 127:46–57. https://doi.org/10.1016/j.schres.2010.12.020

Braak H, Alafuzoff I, Arzberger T, Kretzschmar H, Del Tredici K (2006) Staging of Alzheimer disease-associated neurofibrillary pathology using paraffin sections and immunocytochemistry. Acta Neuropathol 112:389–404. https://doi.org/10.1007/s00401-006-0127-z

Bu B, Li J, Davies P, Vincent I (2002) Deregulation of cdk5, hyperphosphorylation, and cytoskeletal pathology in the Niemann-Pick type C murine model. J Neurosci 22:6515–6525

Byun K et al (2011) Alteration of the CNS pathway to the hippocampus in a mouse model of Niemann-Pick, type C disease. J Chem Neuroanat 42:39–44. https://doi.org/10.1016/j.jchemneu.2011.04.003

Causevic M et al (2018) BACE1-cleavage of Sez6 and Sez6L is elevated in Niemann-Pick type C disease mouse brains. PLoS ONE 13:e0200344. https://doi.org/10.1371/journal.pone.0200344

Distl R, Treiber-Held S, Albert F, Meske V, Harzer K, Ohm TG (2003) Cholesterol storage and tau pathology in Niemann-Pick type C disease in the brain. J Pathol 200:104–111. https://doi.org/10.1002/path.1320

Eickhoff SB, Stephan KE, Mohlberg H, Grefkes C, Fink GR, Amunts K, Zilles K (2005) A new SPM toolbox for combining probabilistic cytoarchitectonic maps and functional imaging data. Neuroimage 25:1325–1335. https://doi.org/10.1016/j.neuroimage.2004.12.034

Eratne D et al (2019) Cerebrospinal fluid neurofilament light chain is elevated in Niemann–Pick type C compared to psychiatric disorders and healthy controls and may be a marker of treatment response Australian & New Zealand. J Psychiatry:0004867419893431. https://doi.org/10.1177/0004867419893431

Evans TE et al (2018) Subregional volumes of the hippocampus in relation to cognitive function and risk of dementia. Neuroimage 178:129–135. https://doi.org/10.1016/j.neuroimage.2018.05.041

First M et al (2002) Structured clinical interview for DSM-IV-TR axis I disorders, research version, patient edition. SCID-I/P, New York, pp 94-1

Geberhiwot T et al (2018) Consensus clinical management guidelines for Niemann-Pick disease type C. Orphanet J Rare Dis 13:50. https://doi.org/10.1186/s13023-018-0785-7

Good CD, Johnsrude IS, Ashburner J, Henson RN, Friston KJ, Frackowiak RS (2001) A voxel-based morphometric study of ageing in 465 normal adult human brains. Neuroimage 14:21–36. https://doi.org/10.1006/nimg.2001.0786

Heitz C, Epelbaum S, Nadjar Y (2017) Cognitive impairment profile in adult patients with Niemann pick type C disease. Orphanet J Rare Dis 12:166. https://doi.org/10.1186/s13023-017-0714-1

Henneman WJP et al (2009) Baseline CSF p-tau levels independently predict progression of hippocampal atrophy in Alzheimer disease. Neurology 73:935–940. https://doi.org/10.1212/WNL.0b013e3181b879ac

Hochberg Y, Benjamini Y (1990) More powerful procedures for multiple significance testing. Stat Med 9:811–818. https://doi.org/10.1002/sim.4780090710

Iturriaga C, Pineda M, Fernandez-Valero EM, Vanier MT, Coll MJ (2006) Niemann-Pick C disease in Spain: clinical spectrum and development of a disability scale. J Neurol Sci 249:1–6. https://doi.org/10.1016/j.jns.2006.05.054

Kesner RP (2018) An analysis of dentate gyrus function (an update). Behav Brain Res 354:84–91. https://doi.org/10.1016/j.bbr.2017.07.033

Kurth F, Cherbuin N, Luders E (2015a) Reduced age-related degeneration of the hippocampal subiculum in long-term meditators. Psychiatry Res 232:214–218. https://doi.org/10.1016/j.pscychresns.2015.03.008

Kurth F, Luders E, Gaser C (2015b) Voxel-based Morphometry. In: Toga A (ed) Brain mapping: an encyclopedic reference, vol 1. Academic Press, London, pp 345–349

Kurth F, Cherbuin N, Luders E (2017a) The impact of aging on subregions of the hippocampal complex in healthy adults. NeuroImage 163.https://doi.org/10.1016/j.neuroimage.2017.09.016

Kurth F, Cherbuin N, Luders E (2017b) The impact of aging on subregions of the hippocampal complex in healthy adults. Neuroimage 163:296–300. https://doi.org/10.1016/j.neuroimage.2017.09.016

Kurth F, Jancke L, Luders E (2017c) Sexual dimorphism of Broca's region: More gray matter in female brains in Brodmann areas 44 and 45. J Neurosci Res 95:626–632. https://doi.org/10.1002/jnr.23898

Kurth F, Cherbuin N, Luders E (2018a) Age but no sex effects on subareas of the amygdala. Hum Brain Mapp. https://doi.org/10.1002/hbm.24481

Kurth F, Jancke L, Luders E (2018b) Integrating cytoarchitectonic probabilities with MRI-based signal intensities to calculate regional volumes of interest. In: Spalletta G, Piras F, Gili T (eds) Brain morphometry. Neuromethods, vol 136. Humana Press, New York. https://doi.org/10.1007/978-1-4939-7647-8_8

Low A, Foo H, Yong TT, Tan LCS, Kandiah N (2019) Hippocampal subfield atrophy of CA1 and subicular structures predict progression to dementia in idiopathic Parkinson's disease. J Neurol Neurosurg Psychiatry 90:681–687. https://doi.org/10.1136/jnnp-2018-319592

Luders E, Kurth F, Toga AW, Narr KL, Gaser C (2013) Meditation effects within the hippocampal complex revealed by voxel-based morphometry and cytoarchitectonic probabilistic mapping. Front Psychol 4:398. https://doi.org/10.3389/fpsyg.2013.00398

Mak E et al (2019) Beta amyloid deposition maps onto hippocampal and subiculum atrophy in dementia with Lewy bodies. Neurobiol Aging 73:74–81. https://doi.org/10.1016/j.neurobiolaging.2018.09.004

Mattsson N et al (2012) Amyloid-beta metabolism in Niemann-Pick C disease models and patients. Metab Brain Dis 27:573–585. https://doi.org/10.1007/s11011-012-9332-8

Muller-Ehrenberg L, Riphagen JM, Verhey FRJ, Sack AT, Jacobs HIL (2018) Alzheimer's disease biomarkers have distinct associations with specific hippocampal subfield volumes. J Alzheimers Dis 66:811–823. https://doi.org/10.3233/jad-180676

Nakahara S, Matsumoto M, van Erp TGM (2018) Hippocampal subregion abnormalities in schizophrenia: a systematic review of structural and physiological imaging studies. Neuropsychopharmacology Reports 38:156–166. https://doi.org/10.1002/npr2.12031

Patterson M (1993) Niemann-Pick Disease Type C. In: Adam MP, Ardinger HH, Pagon RA, Wallace SE, Bean LJH, Stephens K, Amemiya A (eds) GeneReviews(®). University of Washington, Seattle Copyright © 1993–2020, University of Washington, Seattle. GeneReviews is a registered trademark of the University of Washington, Seattle. All rights reserved., Seattle

Rego T et al (2019) Psychiatric and cognitive symptoms associated with Niemann-Pick type C disease: neurobiology and management. CNS Drugs 33:125–142. https://doi.org/10.1007/s40263-018-0599-0

Sevin M, Lesca G, Baumann N, Millat G, Lyon-Caen O, Vanier MT, Sedel F (2007) The adult form of Niemann-Pick disease type C. Brain 130:120–133. https://doi.org/10.1093/brain/awl260

Stampfer M et al (2013) Niemann-Pick disease type C clinical database: cognitive and coordination deficits are early disease indicators. Orphanet J Rare Dis 8:35. https://doi.org/10.1186/1750-1172-8-35

Stav AL et al (2016) Hippocampal subfield atrophy in relation to cerebrospinal fluid biomarkers and cognition in early Parkinson's disease: a cross-sectional study. NPJ Parkinsons Dis 2:15030. https://doi.org/10.1038/npjparkd.2015.30

Steve TA, Jirsch JD, Gross DW (2014) Quantification of subfield pathology in hippocampal sclerosis: A systematic review and meta-analysis. Epilepsy Res 108:1279–1285. https://doi.org/10.1016/j.eplepsyres.2014.07.003

Tavitian A, Song W, Schipper HM (2019) Dentate Gyrus Immaturity in Schizophrenia. Neuroscientist 25:528–547. https://doi.org/10.1177/1073858418824072

Treiber-Held S, Distl R, Meske V, Albert F, Ohm TG (2003) Spatial and temporal distribution of intracellular free cholesterol in brains of a Niemann-Pick type C mouse model showing hyperphosphorylated tau protein. Implications for Alzheimer's disease. J Pathol 200:95–103. https://doi.org/10.1002/path.1345

Villemagne VL, Velakoulis D, Dore V, Bozinoski S, Masters CL, Rowe CC, Walterfang M (2019) Imaging of tau deposits in adults with Niemann-Pick type C disease: a case-control study. Eur J Nucl Med Mol Imaging 46:1132–1138. https://doi.org/10.1007/s00259-019-4273-7

Walterfang M et al (2010) White and gray matter alterations in adults with Niemann-Pick disease type C: a cross-sectional study. Neurology 75:49–56. https://doi.org/10.1212/WNL.0b013e3181e6210e

Walterfang M et al (2011) Size and shape of the corpus callosum in adult Niemann-Pick type C reflects state and trait illness variables. AJNR Am J Neuroradiol 32:1340–1346. https://doi.org/10.3174/ajnr.A2490

Walterfang M et al (2013) Subcortical volumetric reductions in adult Niemann-Pick Disease Type C: a cross-sectional study. Am J Neuroradiol 34:1334. https://doi.org/10.3174/ajnr.A3356

Walterfang M et al (2020) Imaging of neuroinflammation in adult Niemann-Pick type C disease: A cross-sectional study. Neurology 94:e1716–e1725. https://doi.org/10.1212/wnl.0000000000009287

Zervas M, Dobrenis K, Walkley SU (2001) Neurons in Niemann-Pick disease type C accumulate gangliosides as well as unesterified cholesterol and undergo dendritic and axonal alterations. J Neuropathol Exp Neurol 60:49–64. https://doi.org/10.1093/jnen/60.1.49

Zhang M, Wang X, Jiang F, Wang W, Vincent I, Bu B (2010) Mitotic Epitopes are Incorporated into Age-dependent Neurofibrillary Tangles in Niemann-Pick Disease Type C. Brain Pathol 20:367–377. https://doi.org/10.1111/j.1750-3639.2009.00286.x

Zhou S, Davidson C, McGlynn R, Stephney G, Dobrenis K, Vanier MT, Walkley SU (2011) Endosomal/lysosomal processing of gangliosides affects neuronal cholesterol sequestration in Niemann-Pick disease type C. Am J Pathol 179:890–902. https://doi.org/10.1016/j.ajpath.2011.04.017